Zhao, X., Shi, Z., and Chen, Q. 2020. "Inverse design of an indoor environment using a filter-based topology method with experimental verification," *Indoor Air*, 30:1039–1051.

Inverse design of an indoor environment using a filter-based topology method with experimental verification

Xingwang Zhao[1,2], Zhu Shi[2], Qingyan Chen[2,*]

[1]Tianjin Key Laboratory of Indoor Air Environmental Quality Control, School of Environmental Science and Engineering, Tianjin University, Tianjin 300072, China
[2]School of Mechanical Engineering, Purdue University, West Lafayette, IN 47907, USA

[*]*Corresponding email: yanchen@purdue.edu*

ABSTRACT

In order to create a healthy, comfortable, productive, and energy-efficient indoor environment, the computational fluid dynamics (CFD)-based adjoint method with an area-constrained topology method can be used to inversely design the optimal number, size, location, and shape of air supply inlets, and air supply parameters. However, this method is not very mature, and the distribution of retained inlets is always scattered. To solve that problem, this investigation introduced a filter method that smooths the intermediate results during the inverse design process. Using a three-dimensional, non-isothermal, asymmetrical office with pre-set air supply inlets as an example, this study verified the performance of the proposed filter-based topology method. The verified method was then used to solve a multi-objective design problem and design an optimal indoor environment for a room. The results indicate that the proposed method was able to find the optimal number, location, and shape of air supply inlets and the optimal air supply temperature, velocity, and angle that led to a thermally comfortable, healthy, productive, and energy-efficient indoor environment. Finally, this investigation installed the optimal inlets in an environmental chamber to mimic the room. The measured air temperature, velocity, and mean age of air in several typical locations in the environmental chamber matched the CFD simulation results very closely.

KEYWORDS: *Inverse design; Multi-objective problem; Filter-based topology method, Indoor environment; CFD-based adjoint method*

Practical Implications

- This investigation proposed a filter-based topology method for optimal design of the indoor environment and validated it by the experiment.
- The proposed method can be used to design an ideal heating, ventilating and air-conditioning (HVAC) system which create a thermally comfortable, healthy, productive, and energy-efficient indoor environment.
- The HVAC system in the optimal design can be very different from those in the conventional design.

INTRODUCTION

In 2018, 40% of the total primary energy consumed in the United States was in residential and commercial buildings, and nearly 41% of the building energy consumption was for space

heating and cooling[1]. Despite this high energy consumption, the indoor environment is often unsatisfactory with negative effects on work efficiency and the health of occupants. The most common problem is "sick building syndrome" (SBS) [2]. Furthermore, people spend an average of about 21 hours per day indoors[3]. It is crucial to design heating, ventilation, and air-conditioning systems to create an indoor environment that is healthy, comfortable, productive, and energy-efficient[4]; thus, the design of the indoor environment is a multi-objective problem.

For such a problem, the traditional design method uses a trial-and-error process that is unlikely to identify an optimal solution[5]. Moreover, the computational effort increases by several orders of magnitude when the number of design variables increases. Recently, researchers[5, 6] have attempted to use inverse methods to design the indoor environment. The major inverse design methods are the CFD-based genetic algorithm (GA)[6], the CFD-based proper orthogonal decomposition (POD) method[7], the CFD-based artificial neural network (ANN) method[8], and the CFD-based adjoint method[9].

The CFD-based GA method can find the globally optimal solution, but it relies heavily on the choice of samples and requires increased training time to obtain a more accurate solution, especially when the design variables increase in number[6]. In order to reduce the computing time, Wei et al.[7] developed the CFD-based POD method, which is a reduced-order method. It can extract information about the main features of the data from the original complex, high-order nonlinear problems and construct a simple relationship between the design variables and the objective function. This method is not very accurate, but it can significantly reduce the computing time. Meanwhile, the CFD-based ANN method[8] constructs a black-box relationship between the input design variables and the output objective function. Unfortunately, it has the same disadvantages as the CFD-based GA method. To ensure the accuracy of ANN model calculation, one must train the CFD-based ANN method through a large number of samples. In contrast with these approaches, the CFD-based adjoint method[9] as a gradient-based method is very efficient and is independent of the number of design variables. The adjoint method can quickly find the optimal design for a multi-objective design problem, although it may become trapped in local optima. Overall, the adjoint method is the most efficient and suitable method for the inverse design of an ideal indoor environment.

An indoor environment is controlled by many parameters, such as the number, size, location, and shape of air supply inlets, as well as air supply velocity, temperature, and angle. If the design variables are narrowly defined, one will not find the optimal solution. We[10] introduced an area-constrained topology method combined with the CFD-based adjoint method to identify the optimal size, location, and shape of air supply inlets and the optimal air supply temperature, velocity, and angle. The method appeared to design optimal air supplies, but the inlet distribution was scattered. The same problem has appeared in the use of topology optimization for structural design[11, 12, 13]. This scattered distribution has been called the checkerboard phenomenon[14, 15], where wall and inlet cells connect at the corners only. Previous studies[11, 12, 13] have indicated that the checkerboard pattern was not the optimal result but rather a mesh-dependent and numerically unstable result for low-order elements, such as

triangles/tetrahedra or quads/hexahedral elements[16], which influenced the convergence of the flow solution. The phenomenon can be avoided in part by utilizing a higher-order element (polygonal element[17,18]), a mesh regularization strategy[19], or the filter method[20, 21, 22]. In recent decades, the filter method[20, 21, 22] has been widely used in the application of topology optimization to structural design[12,13], to overcome the checkerboard phenomenon[14,15]. For example, the method was employed to design a cantilever beam[16], a Messerschmitt-Bölkow-Blohm (MBB) beam[12], and a pipe bend[23]. However, the method has not been used to inversely design an indoor environment.

Therefore, this study aimed to integrate the filter method and the CFD-based adjoint method with the area-constrained topology, and to explore the performance of the integrated CFD-based adjoint method for multi-objective design problems in the indoor environment.

METHODS

Objective function and its constraints

Our goal was to determine the optimal distribution of inlets, which was the distribution that minimized a pre-set multi-objective function within a pre-set domain using the integrated CFD-based adjoint method. The design objective was a thermally comfortable, healthy, productive, and energy-efficient indoor environment. This study used the predicted mean vote (PMV) index[24] for evaluating thermal comfort. The index is widely used to express the human perception of thermal comfort in the indoor environment. However, the PMV does not account for drafts caused by ventilation, which have been a major concern in office buildings. Therefore, the percent dissatisfied due to draft (PD) index[6] was used to assess the draft sensation. To evaluate indoor air quality (IAQ), this study used the mean age of air τ_p [5, 6]. The lower the mean age of air in a location, the better or fresher is the air quality. Research by Wargocki and Wyon[25] indicated that both thermal comfort and indoor air quality do affect the performance of office work. So, PMV, PD, and age of air will affect the productivity of the occupants in the room. The energy consumption E was determined by:

$$E = A_{inlet} V_{inlet} \rho_{air} C_p \left(T_{outlet} - T_{inlet} \right) \tag{1}$$

where A_{inlet} is inlet area (m^2); V_{inlet} inlet air velocity (m/s); ρ_{air} air density (kg/m^3); C_p specific heat (J/(kg·K)); and T_{inlet} and T_{outlet} inlet and outlet air temperatures (K), respectively.

If the above-mentioned four indexes are used as the design objectives, the corresponding objective functions are f_1, f_2, f_3 and f_4:

$$f_1 = \frac{\int_{\Theta_1} \frac{PMV^2}{PMV^2_{\exp}} \mathrm{d}\Theta_1}{\int_{\Theta_1} \mathrm{d}\Theta_1}; f_2 = \frac{\int_{\Theta_1} \frac{PD}{PD_{\exp}} \mathrm{d}\Theta_1}{\int_{\Theta_1} \mathrm{d}\Theta_1}; f_3 = \frac{\int_{\Theta_2} \frac{\tau_p}{\tau_{p,\exp}} \mathrm{d}\Theta_2}{\int_{\Theta_2} \mathrm{d}\Theta_2}; f_4 = \frac{E}{E_{\exp}} \tag{2}$$

where Θ_1 and Θ_2 are the design domains. Each index in Eq. (2) is normalized by the existing values in the indoor space as a reference.

In the adjoint method, a multi-objective problem must be converted to a single-objective design problem. This study used weighting factors to construct the objective function as:

$$J(\xi) = w_1 f_1 + w_2 f_2 + w_3 f_3 + w_4 f_4 \tag{3}$$

where ξ = ($\mathbf{V}_{inlet}$, T_{inlet}, number, size, locations, and shape) is a vector that denotes the design variables; and w_1, w_2, w_3 and w_4 are weighting factors. The weighting factors for the above four indexes were not from the current studies but from literature[26, 27, 28]. This study used the weighting factors and normalized them. If w_3 and w_4 were zero, the weighting factors for f_1 and f_2 would be 0.455 and 0.545, respectively. These values were derived from a questionnaire[26]. If w_1 and w_4 were zero, the weighting factors for f_2 and f_3 would be 0.53 and 0.47, respectively[27]. Finally, if w_1 and w_2 were zero, the weighting factors for f_3 and f_4 would be 0.57 and 0.43, respectively[28]. Thus, the weighting factors w_1, w_2, w_3 and w_4 should be 0.225, 0.302, 0.27 and 0.203, respectively, after normalization. For an enclosed indoor environment, Reynold number (Re) in the design domain could be small in this study. It was not laminar since turbulence intensity was high. While the Re at the pre-set inlets, as shown in Figure 4(a), was 13000 that was clearly turbulent. Zhang et. al[29] compared different turbulence models for such indoor airflow and found that RNG k-ε model have the best overall performance among the RANS models. Chen[30] also recommended the RNG k-ε model for indoor airflow prediction. So the distribution of air velocity **V** and temperature T in the design domain Θ, as shown in Eq. (2), are controlled by the incompressible, steady-state Reynolds-averaged Navier-Stokes (RANS) equations closed with the RNG k-ε turbulence model[29, 30, 31].

To minimize the objective function in Eq. (3), this investigation used the steepest decent method[32] to update the design variables:

$$\xi_{n+1} = \xi_n - \lambda_n \frac{dJ}{d\xi_n} \tag{4}$$

where ξ_n, ξ_{n+1} are design variables at the current and succeeding design cycles, respectively; n represents the design cycle; and λ is the constant step size. Since the objective function implicitly contains the design variables, we cannot directly calculate the gradient of the objective function over the design variables. Therefore, we have used the CFD-based adjoint method with the adjoint RNG k-ε turbulence model[33] to calculate the gradients. A previous study[33] provides detailed information about the adjoint equations, gradient equations, and adjoint boundary conditions of the CFD-based adjoint method with the adjoint RNG k-ε turbulence model. For identifying the number, size, location, and shape of air supply inlets and the air supply velocity, temperature, and angle, the area-constrained topology[10] method

was the best approach.

Area-constrained topology method

The main idea of area-constrained topology is indirect identification of the number, size, location, and shape of air supply inlets by updating the air supply velocity of each cell independently within the pre-set initial air supply inlet. After a certain number of design cycles, each cell of the initial inlet has a different air supply velocity. The method then adds an area constraint to close those cells with a low given air velocity. However, the final retained inlet distribution is scattered and not concentrated, as shown in Figure 1(a). For simplicity, we[10] only used the centroid-based hierarchical cluster analysis for consolidating these scattered cells, which would change the inversely designed results. For each opening supply inlet as shown in Figure 1 (a), it contains only one grid. The mesh in Figure 1 (a) was the same with the computational mesh which was based on our grid independence test and readers can find the detail information in our previous study[10].

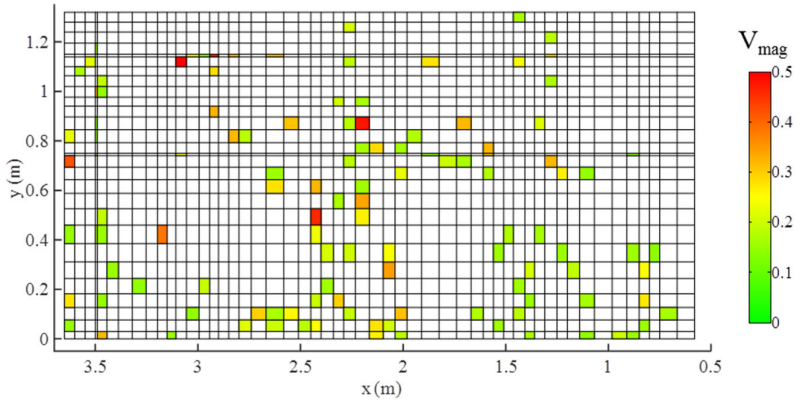

(a)

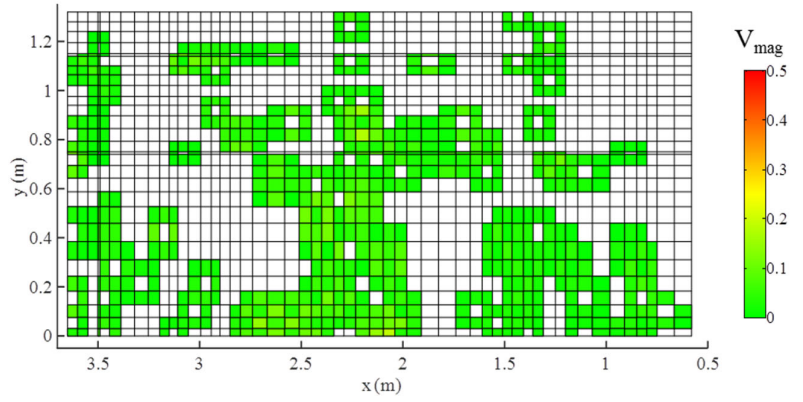

(b)

FIGURE 1 (a) The scattered air supply inlets identified by the area-constrained topology[10] method and (b) the results after using the velocity filter method.

The checkerboard phenomenon usually appears when the topology method has been used to design the optimal structure, which inherits the features of the topology method[34]. However,

the scattered inlets in Figure 1(a) do not exhibit a strict checkerboard phenomenon. One reason may be that we[10] removed too many cells with small velocity, and the summed area of the remaing cells was too small. Other important reasons are mesh dependency and numerical instabilities, which could make convergence difficult. Recently, filters have been widely employed to solve the checkerboard phenomenon[14, 15] and eliminate the dependency of the optimal design on spatial discretization[35, 36, 37].

Filter method

A filter can be regarded as a regularization function for smoothing the distributions of design variables by taking weighted contributions from the neighboring values located within a certain radius. The physical basis of the filter is actually the theory of convolution integrals[19], which are a function used for smoothing data and were originally used in image filtering.

The most frequently used filters are a gradient or sensitivity filter[20] and design variables or a density filter[21, 22]. Sigmund[20] first proposed a gradient filter to prevent rapid variations in design variables, reduce the mesh dependency of topology optimization problems, and facilitate smooth convergence[35, 36, 37]. Since the gradient filter may still be limited by the convergence problem[21], a design variable filter was introduced[21], and the existence of a solution has been mathematically proven[12, 16]. The filter can reduce large contrasts in design variables between two adjacent cells[11, 23, 38]. For example, Figure 1(b) shows the results after we applied the design variable filter. For this study, we used the gradient filter and velocity filter simultaneously. The gradient filter was used to smooth the calculated gradients, and the design variable filter was employed to process the updated air supply velocities.

The gradient filter used in this investigation, as shown in Eq. (5), re-determines the cell gradient according to the adjacent cell gradients in a neighborhood of radius r_0. The weighting factors ω_j are calculated by Eq. (6) as shown in Figure 2. The velocity filter was determined in the same way, as shown in Eq. (7).

$$\frac{\overline{dJ_i}}{d\xi_i} = \sum_{j=1}^{N} \frac{dJ_j}{d\xi_j} S_j \omega_j \Big/ \sum_{j=1}^{N} S_j \omega_j ;\ N_j = \left\{ j \,|\, r_{ij} \le r_0 \right\} \tag{5}$$

$$\omega_j = \frac{\hat{H}_j}{r_0} = \frac{r_0 - r_{ij}}{r_0} \tag{6}$$

$$\overline{\mathbf{V}_{inlet,i}} = \sum_{j=1}^{N} \mathbf{V}_{inlet,j} S_j \omega_j \Big/ \sum_{j=1}^{N} S_j \omega_j \tag{7}$$

where S_i is the area of cell I, r_{ij} the distance between cell i and cell j, N_j neighborhood element j, and $\hat{H}_j$ the convolution operator.

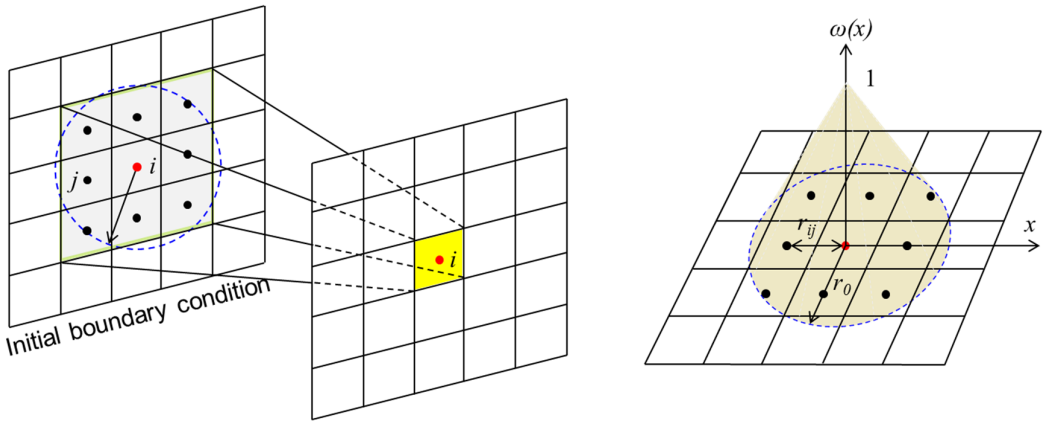

FIGURE 2 The weight function ω(x) for the linear projection scheme.

Note that the original gradients dJ/d$\boldsymbol{\xi}$ and design variables $\mathbf{V}_{\text{inlet}}$ lose their physical meaning. This occurs because the gradients and design variables are redetermined by the filter. The redetermined gradient and velocity, as shown in Eqs. (5) and (7), are always referred to as the physical gradient and velocity that are the solution of the inverse design process[39]. In addition, the solution of the inverse design process can be affected by the filter radius. According to recent studies[11, 12], the proper filter radius can only be determined by a computationally intensive process of trial and error. For this investigation, the proper filter radius was twice the average mesh edge length.

Inverse design process

The integrated CFD-based adjoint method was implemented in OpenFOAM (Open Field Operation And Manipulation)[40], which allows researchers to modify the code according to their needs. Our investigation began the inverse design process as shown in Figure 3 by entering the initialized design variables into the software program, and the integrated adjoint method ran the CFD simulation to evaluate the multi-objective function[41]. If the objective function did not satisfy the convergence criterion, the method calculated the derivative of the objective function J($\boldsymbol{\xi}$) over the design variables $\boldsymbol{\xi}$, so that the method could find the direction in which to adjust the design variables and further minimize the objective function. Since the objective function was controlled by the RANS equations with the RNG k-ε model during the optimization process, this study used the CFD-based adjoint method with the adjoint RNG k-ε turbulence model[33] to calculate the gradients. Next, the gradient filter was used to smooth the gradients. Finally, the study used the steepest descent method[32] to adjust the design variables[42] and applied the velocity filter. The process was repeated until the objective function satisfied the convergence criterion. This criterion was set as $|J_n - J_{n-1}| < \delta$, where J_{n-1}, J_n are the objective function at previous and current design cycles, respectively, and where $n \geq 2$ and $\delta = 10^{-4}$.

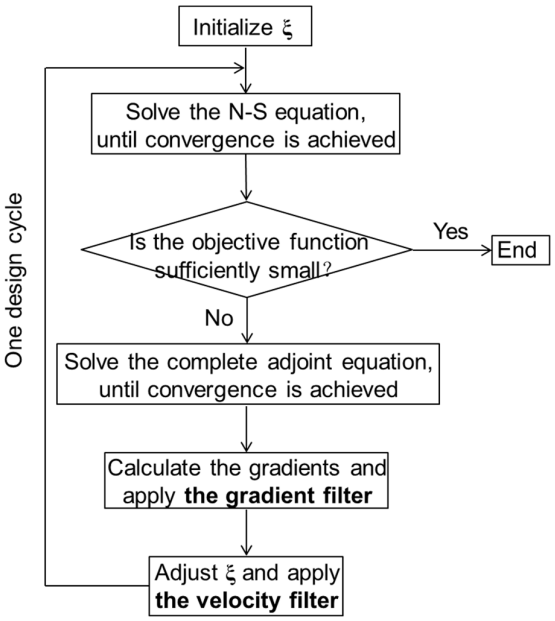

FIGURE 3 The inverse design process of the filter-based topology method.

Experimental methods and instruments

To verify the accuracy of the CFD simulation and the inverse design results, we conducted experimental measurements in an environmental chamber at Purdue University with the inversely designed air supply system. The inverse design process assumed that 100% fresh air was supplied by the HVAC system, and this was also implemented in the HVAC system for the chamber. The experiment measured the air velocity, air temperature, and tracer gas concentration to determine PMV, PD, and the mean age of air.

This study used hot-sphere anemometers to measure the air velocity and air temperature. The accuracy of the devices was ±0.01 m/s for velocity and ±0.3 K for air temperature, and the measurement frequency was 1 Hz. In addition, an ultrasonic anemometer with a measurement error of ±2% and measurement accuracy of 0.005 m/s was used as a reference for measuring the direction and magnitude of the air velocity. A multi-gas monitor and analyzer system was used to measure tracer-gas concentration, and SF_6 was used as the tracer gas because the background concentration of SF_6 was almost zero. This investigation used the step down (decay) method[43] to calculate the local mean age of air τ by

$$\tau = \frac{\int_0^\infty [c(t) - c(\infty)]dt}{c(0) - c(\infty)} \tag{8}$$

where c(t), c(0), and c(∞) are the tracer-gas concentration at t, 0, and infinity, respectively.

Before conducting the experiment, we ran the air-conditioning system for the environmental chamber for more than two hours to stabilize the airflow. During the experiment, we measured the air velocity and air temperature in the middle of the chamber and in the regions

around occupants, since our objective was to design an optimal micro environment around the occupants. The distance between the occupants and the hot-sphere anemometers was 0.1 m. For better comparison with numerical inverse design results, this investigation conducted measurements for 30 min at each point. Repeated experiments were also performed in this study, and all the data was used for analysis. Since the wall temperature during the experiment was different from that used in the inverse design process, we used an infrared thermometer with reading repeatability of ±0.02% of absolute temperature to measure the wall surface temperatures.

RESULTS

To verify the performance of the filter-based topology method, we used it to identify air supply inlets in a three-dimensional room that had been pre-set by forward CFD simulation. The inverse method was then employed to design an optimal air supply system based on a state-of-the-art displacement ventilation design from Shi and Chen[44]. Finally, the performance of the optimal air supply system was compared with CFD and experimental data published by Shi and Chen[44] and with our measurements in the environmental chamber.

Verification of the filter-based topology method

The case used to verify the filter-based topology method was a three-dimensional ventilated office with an asymmetrical layout, as shown in Figure 4(a). The geometry of the office and the sizes and locations of the dummies, personal computers, and tables were the same as in the case with displacement ventilation. This investigation first pre-set two inlets with an air supply velocity of $\mathbf{V}_{inlet}$ = (0.27, 0, 0) m/s and air supply temperature of T_{inlet} = 19 ºC at the bottom of the left wall, as shown in Figure 4(a). And the Re at the pre-set two inlets is 13000. Next, a forward CFD simulation was used to calculate the air distribution. We randomly selected five profiles of air velocity and temperature in the room (the five red lines in Figure 4) as design objectives, and then used the inverse design method to identify the two inlets by specifying the possible region of the inlets as the bottom of the left wall, as indicated by the green area in Figure 4(b). If the filter-based topology method was able to identify the two inlets, then the method would be verified. For this geometric model, we used a structured grid of hexahedral elements with 133,625 cells according to our grid-independence tests. The details information can be found in discussion part, as shown in Figure 14.

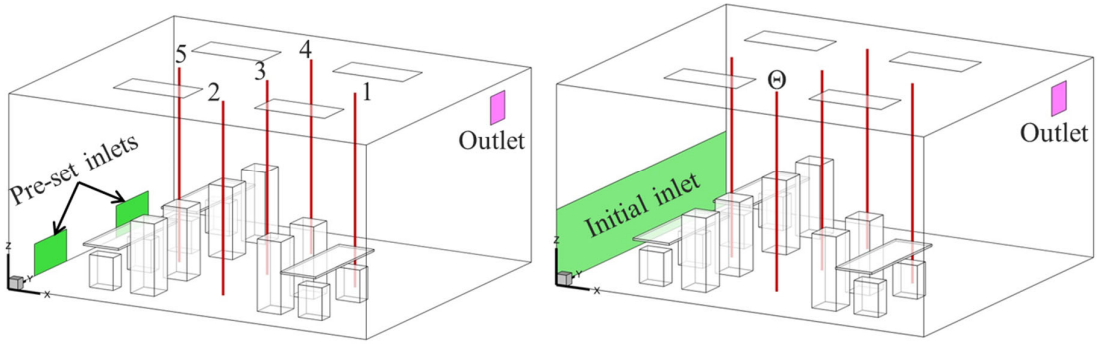

(a) (b)

FIGURE 4 Schematic and design domains Θ of the office

The objective function for the inverse design can be expressed as Eq. (9). The velocity $\mathbf{V}_{0,i}$ and temperature $T_{0,i}$ along the five lines were from the CFD simulation.

$$J(\xi) = w_5 \sum_{i=1}^{m} \left(\frac{\left|\mathbf{V}_i - \mathbf{V}_{0,i}\right|^2}{\left|\mathbf{V}_{inlet}\right|^2} * \frac{vol_i}{vol_{Total}} \right) + w_6 \sum_{i=1}^{m} \left(\frac{\left(T_i - T_{0,i}\right)^2}{\left(T_{max} - T_{min}\right)^2} * \frac{vol_i}{vol_{Total}} \right) \quad (9)$$

where w_5 and w_6 are the weighting factors, assumed to be 0.5 in this investigation; m is the total number of cells in the design domain; V_i and T_i are the air velocity and temperature inversely calculated at the five lines, respectively; vol_i is the volume of cell I; vol_{Total} is the total volume of the cells in the design domain; and T_{max} and T_{min} are the maximum and minimum temperature, respectively, at the boundary.

In the inverse design process, the steepest descent method updated the air supply velocity for each cell in the initial inlet as shown in Figure 5. At the 25th design cycle, the objective function did not decrease, and the convergence criterion was achieved. The design process identified two inlets, although the shapes were not rectangular and the locations were slightly higher than the pre-set ones in red. Figure 6 compares the air temperature and velocity along lines 2, 3, and 4 between the inverse design and the original CFD simulation. The two are very close to each other. Note that the difference could be further reduced if additional lines were used as the design objective. Thus, the filter-based topology method was verified as sufficiently good.

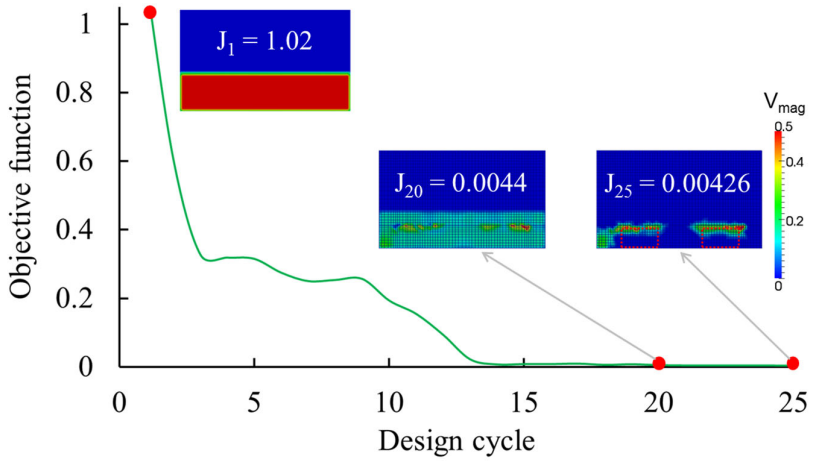

FIGURE 5 Changes in the objective function and air supply inlets with the inverse design process

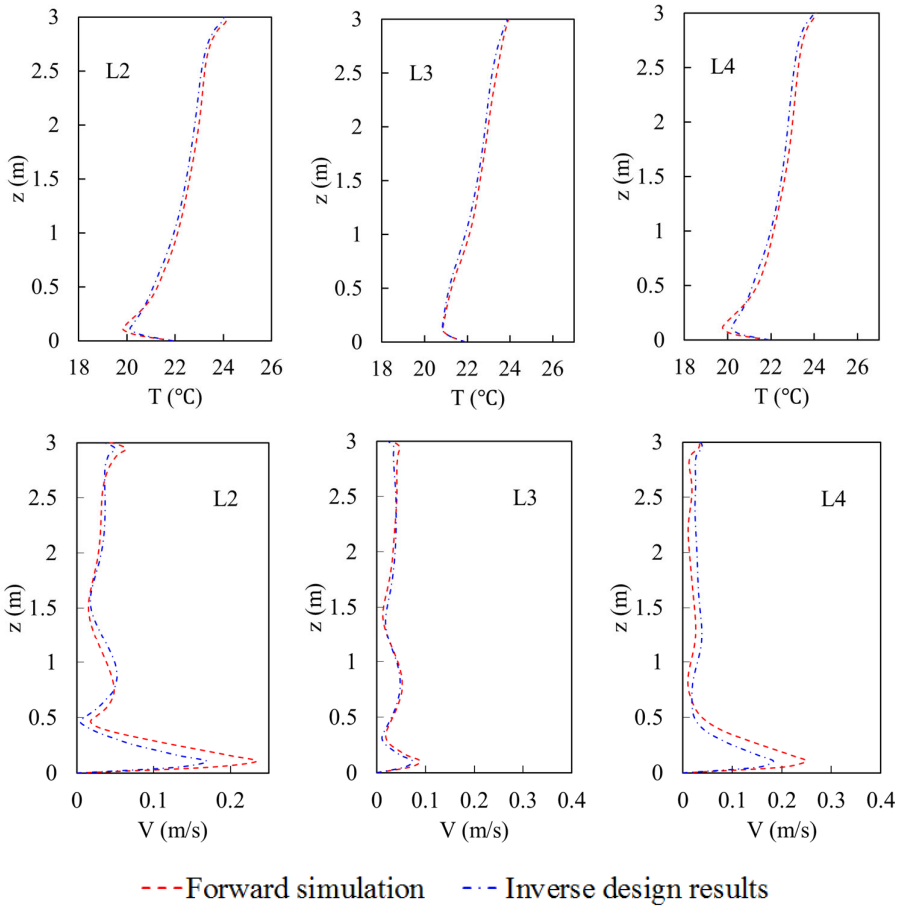

FIGURE 6 Comparison of air temperature and velocity profiles predicted by the forward CFD simulation and the inverse design, where z is the height from the floor

Optimal design of an ideal indoor environment and experimental verification

After verifying the filter-based topology method, this study used it to identify an optimal air supply method for a room as shown in Figure 7. The room was actually an environmental chamber used by Shi and Chen[44] to study displacement ventilation. The displacement ventilation design was the state of the art according to the conventional design approach. Displacement ventilation supplied air to the lower part of the room to improve the air quality, but it also created a vertical temperature gradient that could cause draft. We used the displacement ventilation system as the initial design and combined PMV, PD, the mean age of air, and energy consumption into a multi-objective function with weighting factors, as in Eq. (1), to achieve an optimal design. The design variables were inlet number, size, location, and shape and the corresponding air supply velocity, temperature, and angle. To reduce the computing effort, we assumed that the inlets were in the left-hand wall and the floor, as indicated by the green areas in Figure 7(b) and (c). The initial air supply velocity through the right-hand wall was V_{inlet} = (0.5, 0.1, 0.1) m/s and through the floor V_{inlet} = (0.1, 0.1, 0.5) m/s. The initial air supply temperature was T_{inlet} = 20 ºC. All other boundary conditions were the same as those used by Shi and Chen[44] for displacement ventilation. Design domains Θ_1, as shown in red in Figure 7(b) were used to evaluate PMV and PD and were 0.1 m away from

the occupants. Design domains Θ_2 in Figure 7(c) were used to calculate the local mean age of air in the breathing zones. The convergence criterion was set as $|J_k - J_{k-1}| < 10^{-4}$, where $k \geq 2$. This investigation used a structured grid of hexahedral elements with 275,008 cells to spatially discretize the environmental chamber geometric models according to our grid-independence tests.

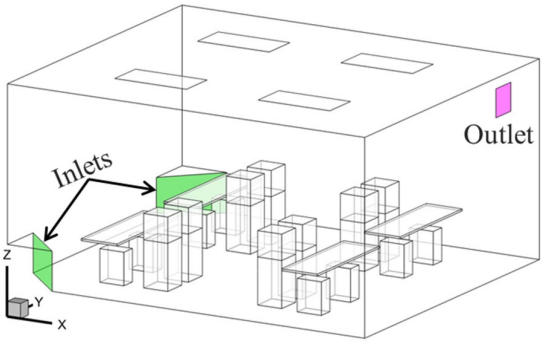

(a) Schematic of the room with displacement ventilation (Shi and Chen[44])

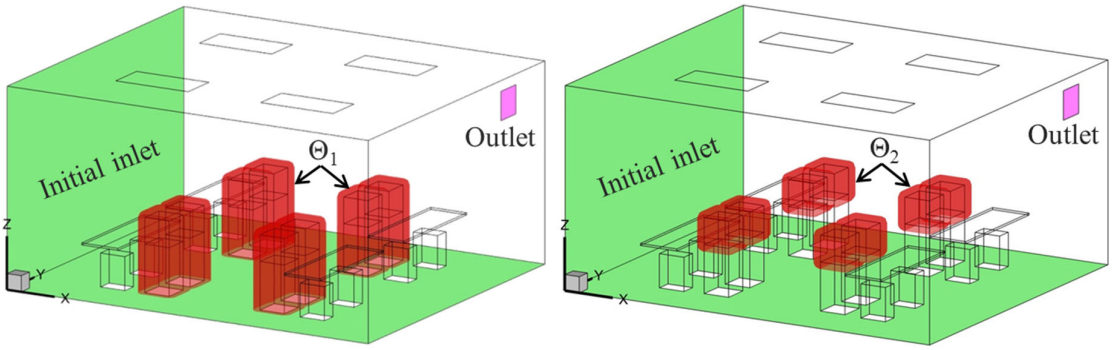

(b) Design domains Θ_1 (c) Design domains Θ_2

FIGURE 7 Schematic of the displacement ventilation system and design domains Θ_1 and Θ_2 used for the optimal design

Figure 8 depicts the design process in which the objective function decreased very quickly during the first 20 design cycles and ultimately reached the convergence criterion at design cycle 50. The figure also shows the change in air supply number, size, location, and shape as well as air velocity. The final results yielded several inlets in the middle of the left wall and several in the floor. For such a small room, it would not be practical to have so many inlets. Applying the cluster method that we had previously proposed[10], we used one long inlet in the left wall and one rectangular inlet in the floor, as indicated by the green area in Figure 9(a). Table 1 provides more detailed information about inlet size and location, and air supply velocity, and temperature.

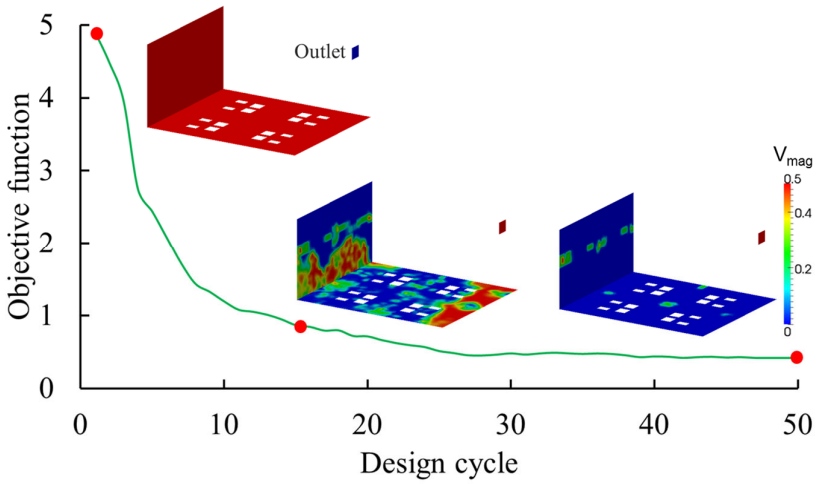

FIGURE 8 Changes in the objective function and air supply inlets with the design cycle for the optimal design

(a) Schematic of the room (b) Environmental chamber

FIGURE 9 (a) Schematic of the air inlets in the room that were identified as optimal by the inverse design process and (b) the environmental chamber.

TABLE 1 Air supply inlet velocity, size, location and Re in the room that were identified for the optimal design

	$V_{x,\,inlet}$ (m/s)	$V_{y,\,inlet}$ (m/s)	$V_{z,\,inlet}$ (m/s)	T_{inlet} (K)	Size (m^2)	Center location (m)	Re
Inlet 1	0.48	0	0	296.25	2.2 × 0.1	(0.0, 1.99, 1.75)	6500
Inlet 2	0	0	0.28	296.25	0.8 × 0.4	(2.8, 3.1, 0.0)	10700

In order to verify the inverse design, this study installed the two inlets in the environmental chamber as shown in Figure 9(b). To achieve a uniform air velocity at the two inlets, we used porous material with a honeycomb structure. As depicted in Figure 10(a), two layers of honeycomb were needed to achieve stable air supply velocity for Inlet 1, and Figure 10(b) shows that one-dimensional air supply was achieved.

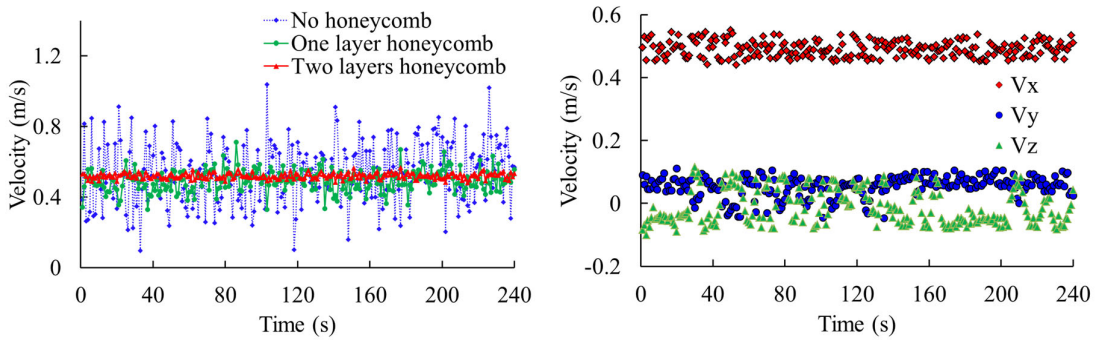

(a) (b)

FIGURE 10 (a) Effect of the honeycomb structure on the air supply velocity and (b) the air supply velocity in three directions from Inlet 1.

In comparison with the displacement ventilation (Shi and Chen[44]), the objective function for the optimal design was improved significantly, as shown in Table 2. In addition, the optimal flow rate (0.195 m^3/s) was almost the same as that for displacement ventilation (0.184 m^3/s), while all the objectives in the optimal design were better than those with displacement ventilation. Thus, the filter-based topology design method exhibits better performance than the conventional trial-and-error method used by experienced designers such as Shi and Chen.

TABLE 2 Area-weighted objectives and objective function in the optimal design

	$\|PMV\|_{avg}$	PD_{avg}	Air_{avg}	E	J(ξ)
Displacement ventilation	0.69	8	230	1.38	1
Optimal design	0.15	5.7	86	0.58	0.42

Figure 11 compares PMV, PD, and the mean age of air around the occupants for the displacement ventilation system and our optimal design. The average |PMV| in the design domain of the displacement ventilation system was 0.69 as shown in Figure 11(a). The thermal comfort level did not satisfy the ISO7730 standard[45], which recommends that the |PMV| be less than 0.5. For the optimal design, Figure 11(b) shows that the average |PMV| in the design domain was only 0.15. Although the average PD with both the displacement ventilation (Figure 11(c)) and the optimal design (Figure 11(d)) was lower than the 15% stipulated by the ASHRAE Handbook[46], the PD around some parts of the occupants with the displacement ventilation was higher than 15%. The mean age of air in the breathing zone with the displacement ventilation, as shown in Figure 11(e), was 230 s, which was fairly young, whereas it was older than 86 s in the optimal design as shown in Figure 11(f). In summary, the optimal design was much better than Shi and Chen's[44] state-of-the-art displacement ventilation system.

(a) PMV with displacement ventilation (b) PMV with optimal design

(c) PD with displacement ventilation (d) PD with optimal design

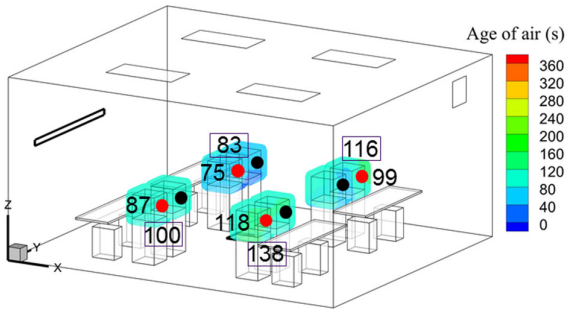

(e) Mean age of air with displacement ventilation (f) Mean age of air with optimal design

FIGURE 11 The PMV (%), PD (%), and mean age of air (s) around the occupants with the displacement ventilation system and the optimal design

Figure 12 compares the air temperature and velocity profiles between the displacement ventilation and our optimal design, in several key locations. The experimental data was available in nine locations. Since the data sets were similar, this paper shows only the results for locations L2, L3, and L4, to save space. Our data includes the minimum and maximum values measured. Meanwhile, Figure 11(f) compares the computed (color cloud) and measured (values in the boxes) local mean age of air in the breathing zones. The measured values for local mean age of air were 15% higher than the computed results. It was difficult to measure the mean age of air since it was obtained through tracer-gas concentration decay. The decay took a long time and thus was subject to variations in many environmental and thermal conditions. Generally speaking, the CFD results matched the experiment data very closely, and therefore all the numerical results presented here are reliable.

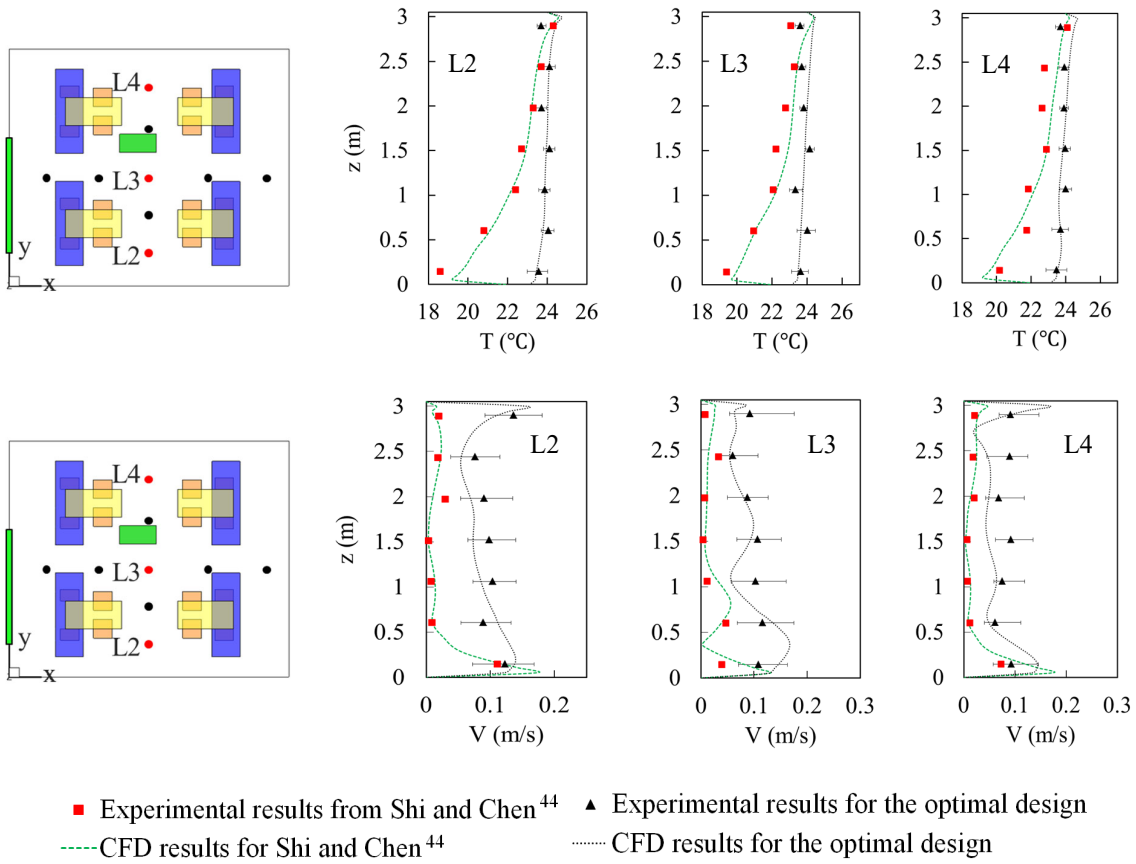

FIGURE 12 Comparison of measured and simulated air temperature and velocity profiles in locations L2, L3, and L4 between the optimal design and displacement ventilation[44], where z is the height from the floor

Figure 12 also shows that the air temperature with the optimal design was higher and more uniform than that with the displacement ventilation. A more uniform temperature could reduce the PD, and a higher temperature could increase the PD. Thus, the optimal design created a more comfortable environment than did the displacement ventilation. However, the optimal design did not involve mixing ventilation. Mixing ventilation would have a very old mean age of air, whereas the optimal design had a very young mean age of air that was caused mainly by the air from the floor inlet. Meanwhile, the high room air temperature could reduce energy consumption, as shown in Table 2. Figure 12 also indicates that the air velocity with the optimal design was higher than with the displacement ventilation, but it was still very low and thus presented no risk of draft.

Next, Figure 13 illustrates the air temperature and velocity distributions from the experimental measurements and CFD simulations around the occupants along positions P1, P2, and P3 in the optimal design. The results show that the computed temperature and velocity along these three positions matched the measured data very well, except for the velocity in the lower part of P2. The discrepancy may have been caused in part by measurement uncertainty, because some equipment on the floor near P2 was not considered in

the CFD simulation. In addition, the airflow direction from the honeycomb was not exactly normal to the inlet surface, as shown in Figure 10(b). When the air supply from Inlet 2 was assumed to be (0.05, 0.05, 0.27) m/s, the velocity in P1 and P2 changed significantly according to our CFD simulation, as shown in Figure 13. The agreement of the air velocity between the CFD simulation with changed air supply and the measured data along P2 is very good. The results not only confirm the reliability of the CFD results, but also demonstrate good air temperature and velocity distribution around the occupants for thermal comfort.

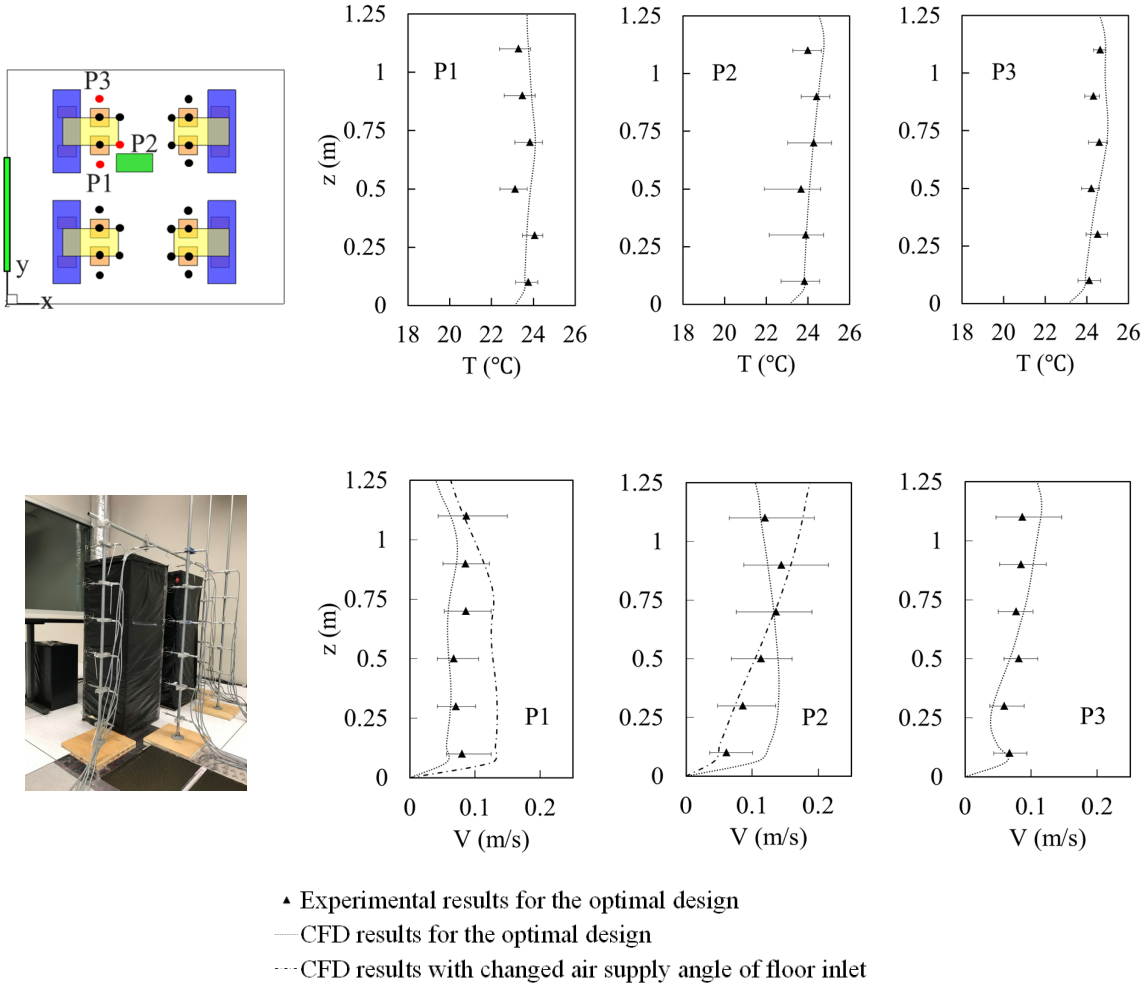

FIGURE 13 Comparison of the air temperature and velocity profiles around the occupants between the CFD simulation and measured data for the optimal design

DISCUSSION

Figure 14 shows the grid independence test for the three-dimensional ventilated office, as shown in Figure 4(a). Except the temperature of the coarse mesh with 18453 cells is larger than other two meshes at the lower part, the temperature profiles of these three different meshes almost the same. For the velocity profiles, the coarse mesh results in most part were different with other two fine meshes. Since the data sets in other lines were similar, this paper only shows the results on line L2 to save space. To reduce the amount of calculations, this

investigation used the mesh with 133625 cells for the further study.

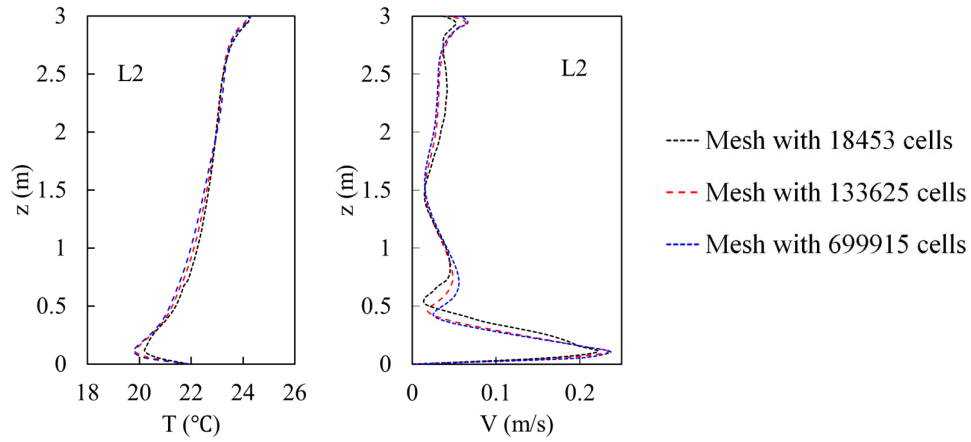

FIGURE 14 Grid independence test for calculation air temperature and velocity profiles on line 2 of the three-dimensional ventilated office, as shown in Figure 4(a)

The inlets identified by the filter-based topology method, as displayed in Figure 5, were not exactly the same as the two pre-set rectangular inlets shown in Figure 4(a). One reason for the difference may be that the continuous adjoint method used in this study provided inaccurate gradients in comparison with the discrete adjoint method[49]. Another possible reason is that this study only used partial information about the flow field to construct the objective function. There would have been multiple solutions to satisfy such partial information, and the adjoint method could easily have been trapped in local optima. It may also be affected by the weighting factors used in Eq. (9). For future study, we will investigate the effect of the discrete adjoint method, different weighting factors, and objective function construction on the inverse design results, and other heuristic algorithms combined with the adjoint method to overcome the inherent disadvantages of the adjoint method.

This study employed only one wall and one floor as potential locations in the optimal design process, and these locations may not have contained the optimal air supply inlets. Setting a larger number of potential locations as the initial inlets might improve the inverse design results. In addition, this study inversely designed the number, size, location, and shape of the inlets only, and did not consider the impact of the outlets. The inverse design process may need to consider inlets and outlets simultaneously.

Since our manuscript focus on studying the performance of the filter-based topology method, we used four indices to construct the objective function. If the number of indices is increased or decreased, the corresponding results, such as the number and size of the inlets and the air supply parameters, would be different.

To achieve perfect agreement between the CFD simulations and experimental measurements is difficult. The simulation used many approximations, and the experimental measurements were not free from errors. In CFD simulations, the grid number and distribution, turbulence

model, and numerical algorithm are very important. In the measurement process, the control of thermo-fluid boundary conditions, experimental method, and equipment are crucial. This investigation did not significantly explore the effects of the CFD and experimental parameters on the accuracy of the results. Doing so would have been difficult, and it was beyond the scope of this investigation. However, these factors deserve serious consideration in the future.

CONCLUSIONS

This investigation proposed a filter-based topology method for optimal design of the indoor environment. The following conclusions can be drawn from this study:

- The filter-based topology method was verified by using it to identify pre-set inlets in a three-dimensional office. The inverse design process correctly identified the two inlets, although the shapes were not rectangular and the proposed locations were slightly higher than the actual ones. The filter-based topology method was sufficiently good for inverse design.

- The filter-based topology method can find the number, size, location, and shape of the air supply inlets as well as air supply velocity, temperature and angle for the optimal design. This design can create a thermally comfortable, healthy, productive, and energy-efficient indoor environment and is better than the state-of-the-art displacement ventilation system designed by the trial-and-error method. The air supply inlet location, size and shape in the optimal design can be very different from those in the conventional design.

- This investigation also conducted experimental measurements of air temperature, air velocity, and the mean age of air in an environmental chamber to validate the optimal design by the filter-based topology method with CFD simulation. The agreement between the CFD simulations and the experimental data was good.

ACKNOWLEDGEMENT

This research was partially supported by the national key project from the Ministry of Science and Technology, China, on “Green Buildings and Building Industrialization” through Grant No. 2018YFC0705300 and the National Natural Science Foundation of China through Grant No. 51478302.

REFERENCES

1. U.S. Department of Energy, 2018. *Buildings Energy Data Book*, Department of Energy, Washington DC.

2. Wargocki P, Wyon DP, Sundell J, et al. The effects of outdoor air supply rate in an office on perceived air quality, sick building syndrome (SBS) symptoms and productivity. Indoor Air. 2000; 10: 222-237.

3. Wallace L. Indoor particles: A review. J Air Waste Manage Assoc. 1996; 46(2): 98-126.

4. Melikov A K. Advanced air distribution: Improving health and comfort while reducing energy use. Indoor air. 2016; 26(1): 112-124.

5. Chen Q, Zhai Z, You X, Zhang T. Inverse Design methods for Built Environment. Routledge, Oxford, England; 2017.
6. Zhai Z J, Xue Y, Chen Q. Inverse design methods for indoor ventilation systems using CFD-based multi-objective genetic algorithm[C]. Build Simul-China. 2014; 7(6): 661-669.
7. Wei Y, Zhang TT, Wang S. Prompt design of the air-supply opening size for a commercial airplane based on the proper orthogonal decomposition of flows. Build Environ. 2016; 96:131-141.
8. Zhang T, You X. A simulation-based inverse design of preset aircraft cabin environment. Build Environ. 2014; 82: 20-26.
9. Liu W, Jin M, Chen C, Chen Q. Optimization of air supply location, size, and parameters in enclosed environments using a computational fluid dynamics-based adjoint method. J Build Perform Simul. 2016; 9(2): 149-161.
10. Zhao X, Liu W, Lai D, Chen Q. Optimal design of an indoor environment by the CFD-based adjoint method with area-constrained topology and cluster analysis. Build Environ. 2018; 138:171-180.
11. Gupta D K, Langelaar M, van Keulen F. QR-patterns: Artefacts in multiresolution topology optimization. Struct Multidiscip O. 2018; 58(4): 1335-1350.
12. Biyikli E, To A C. Proportional topology optimization: A new non-sensitivity method for solving stress constrained and minimum compliance problems and its implementation in MATLAB. PloS one. 2015; 10(12): e0145041.
13. Wang M Y, Zhou S, Ding H. Nonlinear diffusions in topology optimization. Struct Multidiscip O. 2004; 28(4): 262-276.
14. Maute K, Sigmund O. Topology optimization approaches: A comparative review. Struct Multidiscip O. 2013; 6.
15. Riehl S, Friederich J, Scherer M, et al. On the discrete variant of the traction method in parameter-free shape optimization. Comput Method Appl M. 2014; 278: 119-144.
16. Lazarov B S, Sigmund O. Filters in topology optimization based on Helmholtz-type differential equations. Int J Numer Meth Eng. 2011; 86(6): 765-781.
17. Talischi C, Paulino G H, Pereira A, et al. PolyMesher: A general-purpose mesh generator for polygonal elements written in Matlab. Struct Multidiscip O. 2012; 45(3): 309-328.
18. Talischi C, Paulino G H, Pereira A, et al. Polygonal finite elements for topology optimization: A unifying paradigm. Int J Numer Meth Fl. 2010, 82(6): 671-698.
19. Firl M, Wüchner R, Bletzinger K U. Regularization of shape optimization problems using FE-based parametrization. Struct Multidiscip O. 2013; 47(4): 507-521.
20. Sigmund O. On the design of compliant mechanisms using topology optimization. J Struct Eng-Asce. 1997; 25(4): 493-524.
21. Bruns TE, Tortorelli DA. Topology optimization of non-linear elastic structures and compliant mechanisms. Comput Method Appl M. 2001; 190(26-27): 3443-3459.
22. Guest JK, Prévost JH, Belytschko T. Achieving minimum length scale in topology optimization using nodal design variables and projection functions. Int J Numer Meth Eng. 2004; 61(2): 238-254.
23. Kreissl S, Pingen G, Maute K. An explicit level set approach for generalized shape optimization of fluids with the lattice Boltzmann method. Int J Numer Meth Fl. 2011; 65(5): 496-519.

621 24. Fanger PO. Thermal Comfort. Robert E. Kn'cger Publishing Company, Florida; 1982.
622 25. Wargocki P, Wyon D P. Ten questions concerning thermal and indoor air quality effects on
623 the performance of office work and schoolwork. Build Environ. 2017; 112: 359-366.
624 26. Ncube M, Riffat S. Developing an indoor environment quality tool for assessment of
625 mechanically ventilated office buildings in the UK-A preliminary study. Build Environ. 2012;
626 53: 26-33.
627 27. Bohanon Jr H R, Piadé J J, Schorp M K, Saint-Jalm Y. An international survey of indoor
628 air quality, ventilation, and smoking activity in restaurants: A pilot study. J Expo Anal Env
629 Epid. 2003; 13(5): 378-392.
630 28. Yang X B, Jin X Q, Du Z M, et al. Optimum operating performance based online
631 fault-tolerant control strategy for sensor faults in air conditioning systems. Automat Constr.
632 2014; 37: 145-154.
633 29. Zhang Z, Zhang W, Zhai ZJ, Chen QY. Evaluation of various turbulence models in
634 predicting airflow and turbulence in enclosed environments by CFD: Part 2-Comparison with
635 experimental data from literature. HVAC&R Res. 2007; 13 (6):871-886.
636 30. Chen Q. Comparison of different k-ε models for indoor air flow computations. Numer
637 Heat Tr B-Fund. 1995; 28:353-369.
638 31. Yakhot V, Orszag S A, Thangam S, et al. Development of turbulence models for shear
639 flows by a double expansion technique. Phys Fluid Fluid Dynam. 1992; 4(7): 1510-1520.
640 32. Ortega BJM, Rheinboldt WC. Iterative solution of nonlinear equations in several variables.
641 Chap. 8, Academic Press, New York; 1970.
642 33. Zhao X, Chen Q. Inverse design of indoor environment using an adjoint RNG k-ε
643 turbulence model. Indoor air. 2019; 29(2): 320-330.
644 34. Mello LAM, Salas RA, Silva ECN. On response time reduction of
645 electrothermomechanical MEMS using topology optimization. Comput Method Appl M. 2012;
646 247: 93-102.
647 35. Kreissl S. Topology optimization of flow problems modeled by the incompressible
648 Navier-Stokes equations. 2011.
649 36. Kreissl S, Maute K. Levelset based fluid topology optimization using the extended finite
650 element method. Struct Multidiscip O. 2012; 46(3): 311-326.
651 37. Shukla A, Misra A, Kumar S. Checkerboard problem in finite element based topology
652 optimization. International Journal of Advances in Engineering & Technology. 2013; 6(4):
653 1769.
654 38. Andreassen E, Clausen A, Schevenels M, et al. Efficient topology optimization in
655 MATLAB using 88 lines of code. Struct Multidiscip O. 2011; 43(1): 1-16.
656 39. Sigmund O. Morphology-based black and white filters for topology optimization. Struct
657 Multidiscip O. 2007; 33(4-5): 401-424.
658 40. OpenFOAM. The Open Source CFD Toolbox. http://www.openfoam.com, 2012.
659 41. Nielsen P V. Computational fluid dynamics and room air movement. Indoor air. 2004;
660 14(7): 134-143.
661 42. Zhao X, Liu W, Liu S, et al. Inverse design of an indoor environment using a CFD-based
662 adjoint method with the adaptive step size for adjusting the design parameters. Numer Heat Tr
663 A-Appl. 2017; 71(7):707-720.
664 43. Sandberg M, Sjöberg M. The use of moments for assessing air quality in ventilated rooms.

665 Building and environment. 1983; 18(4): 181-197.
666 44. Shi Z, Chen Q. Thermal comfort analysis in a room with displacement ventilation system
667 coupled with passive chilled beams. 5th International High Performance Buildings
668 Conference at Purdue, July 9-12, 2018.
669 47. ISO 7730, 2005. Ergonomics of the Thermal Environment -- Analytical Determination
670 and Interpretation of Thermal Comfort Using Calculation of the PMV and PPD Indices and
671 Local Thermal Comfort Criteria, *International Organization for Standardization*, 7730.
672 48. ASHRAE, 2011. ASHRAE Handbook - HVAC Applications (SI). *American Society of*
673 *Heating, Refrigerating and Air Conditioning Engineers*, Atlanta.
674 45. Li Y, Sandberg M, Fuchs L. Vertical temperature profiles in rooms ventilated by
675 displacement: Full‐scale measurement and nodal modelling. Indoor Air. 1992; 2(4):
676 225-243.
677 46. Melikov A, Pitchurov G, Naydenov K, Langkilde G. Field study on occupant comfort and
678 the office thermal environment in rooms with displacement ventilation. Indoor air. 2005; 15:
679 205-214.
680 49. Towara M, Naumann U. A discrete adjoint model for OpenFOAM. Procedia Computer
681 Science. 2013; 18: 429-438.